Journal of Engineering for Gas Turbines and Power. Received June 19, 2016;
Accepted manuscript posted October 11, 2017. DOI:10.1115/1.4037861

Volume 140, Issue 3,
Article number 032501
March 2018

Transient Thermal Modelling of Ball Bearing Using Finite Element Method

Thierry Sibilli*

*Rolls-Royce Deutschland Ltd & Co KG, 11 Eschenweg, Dahlewitz, Blankenfelde-Mahlow, 15827 Germany

Uyioghosa Igie

School of Aerospace Transport and Manufacturing, Cranfield University, Cranfield, Bedfordshire, MK43 0AL UK

*Moved to: Rolls-Royce UTC in Thermal Management, School of Mechanical Engineering Pusan National University 30 Jangjeon-Dong, Geumjeong-Gu Busan, Korea, 609-735

ABSTRACT

Gas turbines are fitted with rolling element bearings, which transfer loads and supports the shafts. The interaction between the rotating and stationary parts in the bearing causes a conversion of some of the power into heat, influencing the thermal behaviour of the entire bearing chamber. To improve thermal modelling of bearing chambers, this work focused on modelling of the heat generated and dissipated around the bearings, in terms of magnitude and location, and the interaction with the components/systems in the bearing chamber. A thermal network model and a finite element model of an experimental high-pressure shaft ball bearing and housing were generated and a comparison to test rig results have been conducted. Nevertheless, the purpose of the thermal matching process that focused on the finite element model and experimental data is to provide a template for predicting temperatures and heat transfers for other bearing models.

The result of the analysis shows that the predictions of the thermal network are considerate, despite the simplifications. However, lower relative errors were obtained in the finite element model compared to the thermal network model. For both methods, the highest relative error is seen to occur during transient (acceleration and deceleration). This observation highlights the importance of boundary conditions and definitions: surrounding temperatures, heat split and the oil flow, influencing both the heat transfer and heat generation. These aspects, incorporated in the modelling and benchmarked with experimental data, can help facilitate other related cases where there is limited or no experimental data for validation.

INTRODUCTION

Jet engines are fitted with bearings which ensure efficient transmission of the mechanical power. Nevertheless, these components convert part of this power into heat, through the friction caused by the interaction between the moving and stationary parts. Friction resistance is generated at several interfaces inside the bearing and represents the main source of wasteful power. This mechanism leads to a local increase of the metal and oil temperatures, as well as thermal gradients, affecting the operability of the system. This is of interest for the bearing design and manufacture but also to determine the lubricant operating life. The design of the bearing should satisfy the different flight segments of operation and their respective operational power/load requirements with an eye to the system lifespan. This brings about the need for improved thermal predictions in terms of magnitude and spatial resolution and this study is a step in improving the thermal modelling in similar working conditions.

Conventional bearings require lubrication to avoid contact between the static and rotating component parts. The relative speed inevitably produces power losses that are absorbed by the oil itself and transferred as heat to the system via momentum, conduction, convection and radiation (smaller extent). To model these heat transfer mechanism, various thermal management modelling techniques can be applied, however presenting a different level of accuracy and computational demand. The methods include the analytical approach based on Thermal Network Method (TNM) and numerical approach using Finite Element Method (FEM). TNM is based on the discretization of a system with nodes and conductances analogous to approaches in an electrical network [1], alongside the prevailing heat-transfer mechanism, described by their equations.

This approach has a rapid computational time due to the simplification of heat exchanges; being based on the assumption of one-dimensional geometries, applicable to steady-state and no load zone variation. Harris [2] shows a steady-state thermal resistance approach on a roller bearing assembly, highlighting the limitations. Pouly et al. [3], again using the TNM, focus on the power losses in high-speed bearings, with emphasis on the rolling friction and drag forces losses, aside from other sources of power losses. The referred study demonstrates that the overall power losses obtained are comparable to other approaches when adjustments are made on the air fraction in the lubricant. The study also highlights the sensitivity of temperature distribution that is dependent on heat source localisation. This is shown to vary from 70% to 100% and dependent on how the power losses are defined when predicting the heat absorbed by the oil [3].

When the desired resolution is not matched by the thermal network, directly solving the energy equations can increase the accuracy of the model. However, due to the nature of the heat equations, these can only be solved analytically for simple geometries; in the case that a transient solution is required. In the first part of a recent paper, Hannon [4] proposes an upgraded analytical steady-state model based on a system-like approach that takes into

account the interaction between the ball and some of the other components in a bearing chamber. The analytical heat transfer model presented is an integral transform method that incorporates partial differential equations and analytical expressions. The resulting solution presented in the third part series of the study in Hannon et al. [5] shows good agreement in predicting the oil exit temperatures in comparison with the experimental case. The result shows about 1°C deviation in average temperatures from the experimental.

When a transient solution is needed and the complexity of the geometry requires higher spatial resolution, FEM solvers are more suitable. Moreover, they can be easily coupled with other tools to further increase their accuracy. For example, a thermal FEM model can be converted into a thermo-mechanical FEM model able to calculate both thermal and mechanical deformations. Moreover, due to the nature of the problem, a transient solution is required to evaluate the thermal behaviour of the bearing during critical phases like take-off and rapid spool down, when the thermal gradients are more significant. To approach this, the present study begins with a description of the experimental Isolated Bearing Chamber (IBC) and provides a comparison with the predictions using TNM. Further to this, the experimentally predicted temperatures are matched as closely as possible with an equivalent FE model. The purpose of this thermal matching process is to provide a template for predicting temperatures and heat transfers for other bearing models with limited or no experimental data for validation. This framework is illustrated in Fig. 1. This is an effort to improve thermal modelling of bearing chambers, focused on the heat generation and dissipation close to the bearings (in terms of magnitude and location, and the interaction with the components/systems in the bearing chamber).

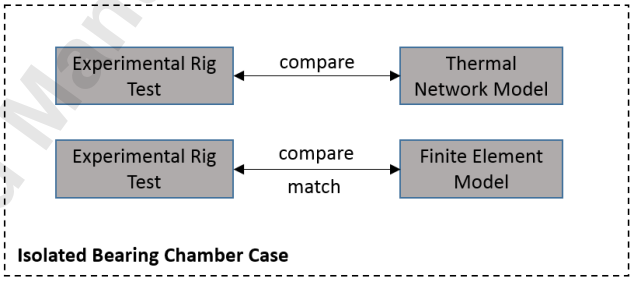

Fig. 1 Framework of the study

EXPERIMENTAL TEST RIG

An experiment test rig was set-up in-house, as described in the internal report of Rolls-Royce [6]. The IBC for a HP compressor was operated under conditions indicative of actual operations in service. The main features and specifications of the test facility are summarised in Table 1. The test rig also consists of 3 flowmeters, 11 accelerometers, 1 load cell and 12 strain gauges, deployed in obtaining and verifying the specification indicated. A square cycle that

consists of four mission segments such as idle, acceleration, full power and deceleration and idle (but five operations) was performed. The idle state and the full power operations are related to steady-state conditions described in Table 2, respectively.

Table 1 Main specifications of experimental rig

Feature	Value
Installed Power	2MW
Hydraulic engine	250kW
Air mass flow	0.5kg/s, variable
Air temperature	573K maximum, variable
Air pressure	500kPa maximum, variable
Oil mass flow	0.67l/s, variable
Oil temperature	423K minimum, variable
Rotating speed	14,600rpm maximum, variable
Radial load	25kN maximum, variable
Axial load	150kN maximum, variable
Dynamic load	16kN maximum, variable

Table 2 Rig test operating conditions

Parameters	Condition 1	Condition 2
Speed (rpm)	7,000	13,000
Axial load (kN)	10	100
Oil inlet temperature (K)	323	323
Oil flow (l/s)	0.075	0.2
Air temperature (K)	513	513

During the test, oil and air flows were chosen to replicate engine environment and the bearing was subject to an axial load that is representative of the interaction with the intermediate casing and the HP compressor. Figure 2 shows three thermocouples located close to the ball-raceway interfaces. Each discrete point represents a group of thermocouples which have the same longitudinal and radial positions but are evenly split in the circumferential direction. With multiple thermocouples at different circumferential angles, it was possible to account for the potential 3D effects in the recorded experimental data. Hereafter, local thermal influences such as the impact of a single and isolated lubricating channel in a particular position can be taken into account, and an enhanced value can be used for the validation of the 2D model. However, the validation exercise was based on an average of all the circumferential thermocouples. All thermocouples recorded measurements at the same frequency of 1 Hz for consistency during

transient operations: when the parameters typically change very quickly. Nevertheless, the measurements from thermocouple M11 showed a high level of noise. This non-controlled phenomenon was even more marked at high speed, which is attributed to a rotor imbalance. As a result, the measurements were post-processed and filtered before using them in the analysis. This procedure resulted in an uncertainty band of ± 5K. For the subsequent part of the study, the main parameters recorded and evaluated during the test for the thermal model included the oil inlet and outlet temperatures, air seal mass flow, pressure of the frontal and rare cavities and the temperature of the frontal and rare cavities.

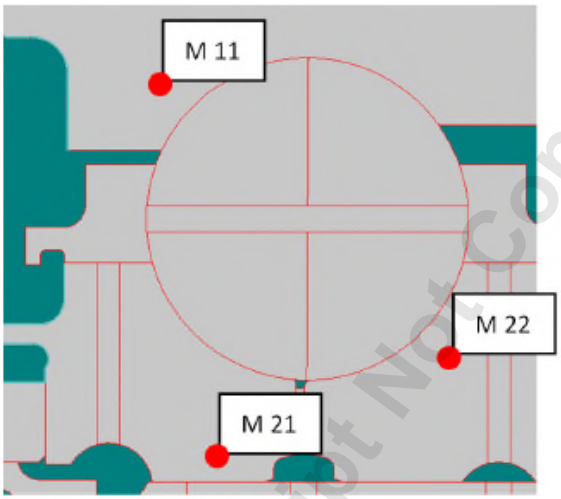

Fig. 2 Thermocouple positions around the ball bearing

THERMAL NETWORK MODEL

As previously described, TNM is based on analytical equations solved for a discrete number of nodes that represent the main components, media and mechanisms of heat exchange that characterize a bearing chamber. In accordance with the approach presented in Pouly [3], the following additional assumptions/limitations:

- Thermal effects of the cage are not taken into account
- Heat generated is modelled at two single points at the ball-raceway interfaces

The thermal network was generated by splitting the bearing into several nodes including the upper and lower races, the balls, the shaft and the bearing housing.

Figure 3 shows the thermal network architecture, with the corresponding node locations in the bearing chamber. All thermal flows are marked in red and the indexes $Q\_$ represent the heat transferred between two nodes while thermal resistances are represented by the symbol R. As for Q_{in} and Q_{out} (in blue), they are the system boundary conditions and are the amount of heat injected into and evacuated from the thermal network respectively. The nodes allow discretizing the ball bearing in domains which are at uniform temperature. In particular, the temperature recorded in proximity to the

bearing was treated as a boundary condition at nodes 1 and 7, to take into account the surrounding geometry not included in the model. Nodes 2 and 6 are used to evaluate the temperature in the outer and inner races respectively, whereas the nodes 3 and 5 were positioned at the balls-races contact to apply the heat generation terms.

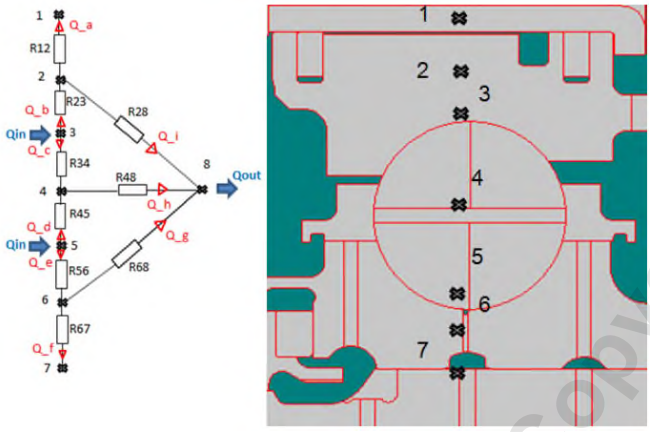

Fig. 3 Node locations on bearing chamber and thermal network

Node 4 accounts for the lubricating fluid in the ball bearing and sets the thermal gradient for the convective exchange between the metal and the oil. The model is limited to 8 nodes to ensure a reasonable number of equations. The thermal analysis is based on the conservation of energy balance, which states the conservation of the total energy for an isolated control volume is constant. In the network, this law is applied to every node and represented by the following set of linear equations in Equs. 1 to 6. This is resolved by linear calculations based on the inverse matrix.

$$Q_b = Q_a + Q_i \quad (1)$$

$$Q_{in} = Q_b + Q_c \quad (2)$$

$$Q_c + Q_d = Q_h \quad (3)$$

$$Q_{in} = Q_d + Q_e \quad (4)$$

$$Q_e = Q_f + Q_g \quad (5)$$

$$Q_i + Q_h + Q_g = Q_{out} \quad (6)$$

The heat generated is quantified using a Rolls-Royce empirical correlation similar to the one presented in Flouros [7]. The heat generated by a bearing is the sum of the different effect, including sliding, spinning and viscous effects [8] and the correlation presented by Flouros [7] captures all these effects in one empirical correlation in this form:

$$H = 1.50674 * 10^{-9} D^{1.11} N^{1.3855} \nu^{0.0525} F_x^{0.2152} \quad (7)$$
$$(V_{oil})^{0.3831} (2.25X^2 - 1.5068X + 7.0221)^{0.761}$$

The Rolls-Royce equation presents similar variables, like diameter, rotational speed, axial force and oil flow and it has been derived for similar applications (i.e. similar D x N range), however presenting few different limitations. In particular, the validity of the correlation is extended to higher oil flow and higher loads and is therefore applicable to this case. Heat removed by the oil is estimated with an energy balance (Eq. 8) in the lubricant itself thanks to the mass transport equation in Holman [9].

$$Q_{out} = W_{oil}(Cp_{oil.out}T_{oil.out} - Cp_{oil.in}T_{oil.in}) \qquad (8)$$

Where Q_{out} is the heat removed by the oil, W_{oil} is the mass flow, $Cp_{oil.out}$ and $Cp_{oil.in}$ are the corresponding heat capacity at the outlet temperature $T_{oil.\mathrm{out}}$ and inlet temperature $T_{oil.\mathrm{in}}$. The nodes of the thermal model are linked together through thermal resistances. All thermal fluxes are subject to a specific resistance which depends on the heat transfer mode and the geometry. The thermal conductance for non-cylindrical components was taken from different sources as shown in Table 3. The complete list of the parameters is available in the referenced study. It is, however, important to point out that a. and b. (half dimensions of the elliptical contact at the ball-raceway interfaces) were calculated using the method presented by Harris [2].

Convective transfers are mainly based on empirical correlations related to the local Nusselt number which takes into account different phenomena which influence the heat transfer. The convective transfer between the ball and the lubricant is modelled as a thermal exchange of an isolated sphere inside a flow [9] through the estimation of the fluid viscosity at the bulk and wall temperatures. The heat transfer coefficients at the oil exit are modelled with different correlations for rotating concentric cylinders separated by a fluid (Taylor-Couette flow) [8], due to the dissimilar rear and front gaps. Table 4 summarizes the empirical correlations.

Table 3 Conduction correlations for the different nodes

Conductance	Expression	Equ
$R_{234} = R_{23} + R_{34}$ [3], [10]	$R_{234} = \frac{\ln(\frac{R_2}{R_3})}{2\pi k\ \Delta x_{o.r}} + \frac{0.918}{2b_{o.r}\sqrt{2a_{o.r}}\ \sqrt{V}} + \frac{\ln(\frac{D}{2})}{2\pi k\ \Delta x_{ball}}$	(9)
$R_{456} = R_{45} + R_{56}$ [3], [10]	$R_{456} = \frac{\ln(\frac{D}{2})}{2\pi k\ \Delta x_{ball}} + \frac{0.918}{2b_{i.r}\ \sqrt{2a_{i.r}}\ \sqrt{V}} + \frac{\ln(\frac{R_5}{R_6})}{2\pi k\ \Delta x_{i.r}}$	(10)
R_{67} [9]	$R_{67} = \frac{1}{\Delta x_{int}}\left(\frac{R_6 - R_{int}}{k_6} + \frac{1}{h_C} + \frac{R_{int} - R_7}{k_7}\right)$	(11)

Table 4 Convection correlations for the different nodes

Convection	Expression	Equ
Ball to oil [9]	$Nu = (1.2 + 0.53Re_D^{0.64}) \times Pr^{0.3}\left(\frac{\mu\|T_{bulk}}{\mu\|T_{wall}}\right)^{0.25}$	(12)
Front gap [8]	$Nu = 0.42\ (TaPr)^{0.25}$	(13)
Rear gap [8]	$Nu = 0.092\ (TaPr)^{0.25}$	(14)

In the outer part of the ball bearing, the thermal resistance Rth_{12} must account for the presence of the squeeze oil film. Figure 4 shows the mix of conduction and convection modelled in R_{12}.

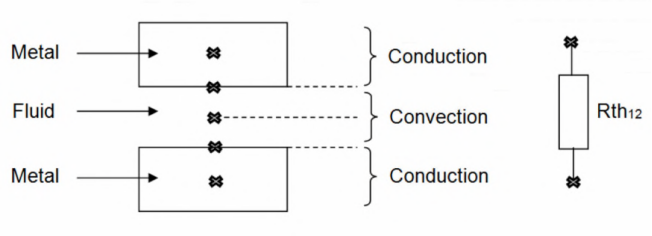

Fig. 4 Thermal exchange at R_{12}

Combining the thermal conduction and convection equations for a cylinder [2] [10], the overall thermal resistance can be expressed by the following equation

$$R_{12} = \frac{1}{\Delta x}\left[\frac{\ln(\frac{R_1}{R_{gap}})}{2\pi k} + \frac{2}{h_{o.film}} + \frac{\ln(\frac{R_{gap}}{R_2})}{2\pi k}\right] \quad (15)$$

Where R_{12} is the overall thermal resistance, Δx is the longitudinal dimension of the gap, $R.$ the different radii at the specified nodes, k is the thermal conductivity of the surrounding materials, and $h_{o.film}$ is the oil side heat transfer coefficient. This parameter is calculated from the Nusselt number in Equ 16 which is estimated through an empirical correlation [9].

$$Nu^{1/2} = 0.6 + 0.387\left[\frac{GrPr}{\left(1 + \left(\frac{0.559}{Pr}\right)^{9/16}\right)^{16/9}}\right]^{1/6} \quad (16)$$

Comparison between Experiment and TNM

The temperatures measured during the experimental test have been subsequently compared with the values calculated from the TNM for the same locations as a function of time along the square cycle. These locations are M11 and M21 only, as M22 is considered to be positioned at the same node, thereby giving identical results due to the limited

number of nodes in the TNM. The comparison between these two methods is presented in Figs 5 and 6 for M11 and M21 locations respectively.

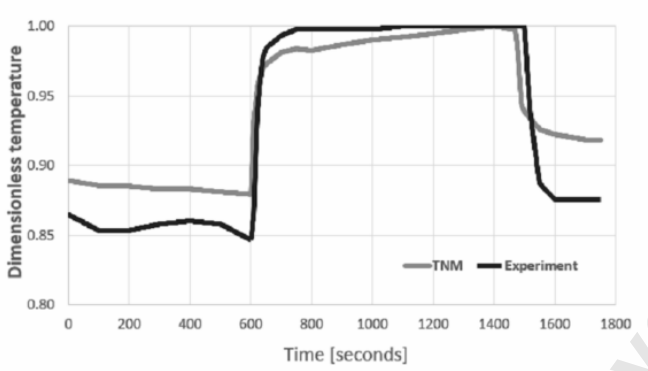

Fig. 5 Experimental and TNM dimensionless metal temperature in M11 location

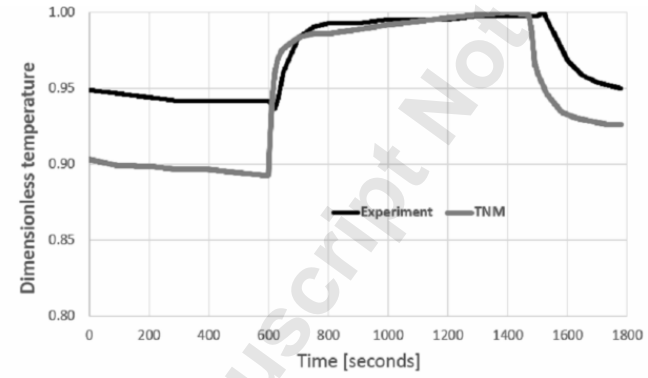

Fig. 6 Experimental and TNM dimensionless metal temperature in M21 location

Figure 5 shows the dimensionless temperature, which is the actual temperature divided by the measured maximum temperature in the cycle. The maximum temperature obtained in the cycle is few seconds before deceleration, where the dimensionless temperature is 1.00, however the test article was considered thermally stabilized as only subject to less than 1% temperature variation in 400s. The first 10 minutes (600 seconds) is the first idle and this relates to condition 1 on Table 2. Subsequent to this is acceleration that takes about 2.7 minutes that is followed by high load that last for 12 minutes (ending at 1484 seconds as shown in the figure). This approximately constant high load condition relates to condition 2 on Table 2. It is followed by a deceleration and ends with a final idle condition. Figure 6 shows that of the M21 location, in agreement with the M11 location, however generally higher dimensionless temperatures at idle.

Figure 7 shows the relative error of the TNM in relation to the experimental test results for both locations. This shows that the highest error occurs during the acceleration for both locations. This is about 8% and 9.5% for M11 and

M21 locations respectively. It is attributed to the sudden flow variations in the bearing chamber during acceleration, caused by rapid changes in rotational speed and axial load. Given the low level of complexity of the TNM, the results obtained overall, are considered satisfactory. Operations with relatively small variation in load show smaller fluctuations in the relative error.

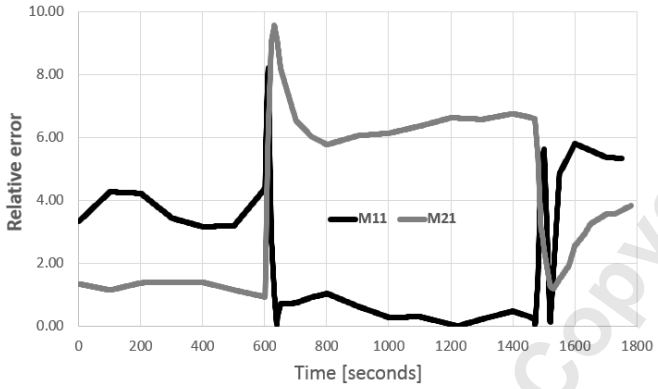

Fig. 7 Error between experimental and TNM dimensionless temperature in M11 and M21 locations

It is however, important to observe that for both locations, M11 has a higher relative error at idle but comparatively lower values at maximum high load. The opposite is the case for location M21, that shows higher errors, explained by the absence of oil feeding channel in the inner ring. Hence, the convective exchange between the inner ring and the oil is neglected with a consequent increase in the overall predicted temperature. Nevertheless, the initial aim of TNM was not to accurately predict the temperature around the bearing but only to roughly quantify the order of magnitude of the heat transfer rate in the local surroundings. For acceleration, the relative error reduces for both locations, however increases to higher values at the final idle condition.

FINITE ELEMENT MODEL

The FEM was implemented on an in-house code that uses a finite element discretization in space and a finite difference discretization in time. This leads to repeatedly solving a non-linear implicit system of equations for the temperatures at the end of each time step. The time stepping errors in the calculated temperatures are estimated and if they are within the requested accuracy, the solution moves on to the next step and if not, the time step is reduced and the step is re-analysed. Combining the energy equation based on the Fourier's law with a linear approximation of the temperature variation within a time step gives the following time matching equation [11]:

$$\left(\frac{M}{\Delta t}+\theta K\right)T_2=\left(\frac{M}{\Delta t}-(1-\theta)K\right)T_1+P \qquad (17)$$

Where *M* is the specific heat matrix, *K* is the conductivity matrix, *P* is the vector of nodal heat flows into the domain and *θ* is the time stepping coefficient. Imposing θ = 0 gives an explicit forward difference algorithm [11] in which the global conductivity matrix does not have to be formed. This method is unstable for times steps greater than a small critical value determined by the smallest element size and is only practical for short scale thermal shock problems modelled with first order elements and a lumped specific heat matrix. A value of θ of 0.5 gives a central difference, or Clark-Nicholson [11], scheme which is unconditionally stable for linear problems and has the greatest accuracy but can produce oscillatory solutions if non-linear boundary conditions are present. Finally θ = 2/3 and θ =1 are respectively the Galerkin and backwards Euler schemes that control spurious oscillations better than the Crank-Nicholson method but at the expense of time step size for a given accuracy [11]. For the subsequent calculations, a value of 0.8 was selected based on the best practice [12]. The residuals of the equation can be written as:

$$R=P+\frac{M}{\Delta t(T_1-T_2)} -K((1-\theta)T_1+\theta T_2) \qquad (18)$$

To solve this equation, a quasi-Newton method is implemented in which the Jacobian is taken as shown in Equ. 19 and iteratively solved imposing the boundary conditions.

$$\frac{\partial R}{\partial T_2}=\frac{\partial P}{\partial T_2}-\frac{M}{\Delta t}-\theta K \qquad (19)$$

Those boundary conditions are similar to the one used for the TNM but due to the nature of the FEM model, the BCs can be further refined to include additional effects. The first advantage is that by using a FEM model it is possible to consider that for this particular application, an axial load from the HP compressor is applied towards the front of the engine and that the balls will exchange load on the front side for the outer race and back side for the inner race, causing an uneven heat conduction and generation. Additionally, it is possible to consider that the bearing is fed by oil in different locations, at a frontal, mid and rear longitudinal positions as shown in Fig. 8. The flow was assumed to be delivered to the nozzles at an equal amount. As indicated previously, there is also an oil flow that feeds the squeeze film, which might influence the bearing temperature, this can also be taken into consideration. Note that the flow split, and directions

are assumed, given that only a detailed analysis/test (2 phase CFD/rig) out of scope for this study, can correctly evaluate them. Flourus [7] showed that uneven flow strongly affects the heat generation and temperature distribution. Further studies should focus on this.

Taking into account all these considerations it was assumed that conduction and convection heat transfers are distributed based on the scheme shown in Fig. 9. Note that only thermal transfers close to the bearing are shown, considering the aim of the study. This figure indicates that all surfaces in contact with the fluid (represented in red) are modelled through the convective mode whereas the parts with the ball-raceway contacts where there is a predominance of conduction, thin oil layer, are represented in blue. The values of conductive and convective heat transfer coefficients are the same as that of the TNM obtained from the equations in Table 3 and 4 respectively.

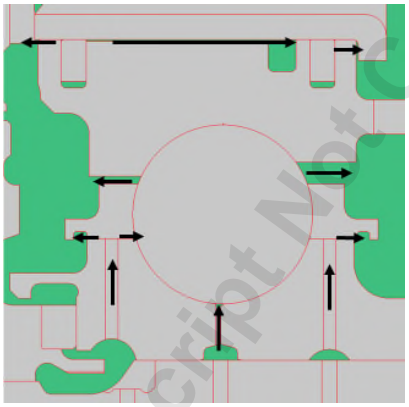

Fig. 8 Oil flows around the bearing

As mentioned before the heat generated by a bearing is the sum of the different effect, including sliding, spinning and viscous effects [9] and the magnitude of these components varies with the location of the bearing due to the thickness of the oil film approaching the contact area [4]. To simulate this effect, it was assumed that 60% of the heat was generated in the loaded ball-raceway section where the contact area is located and related to the direction of the axial load. The other 30% of the heat generated was applied on the unloaded side. This is to take into account that the frictional effects around the contact areas, resulting in an uneven split between the interfaces (due to the different characteristics of the gaps that evolve under the influence of the axial load). The remaining 10% of the heat was applied to the surface of the balls in order to represent the windage due to the rotation of the balls. It is important to point out that the split was kept constant for the entire cycle, so not dependent on speed.

The magnitude of the heat generated by windage variated accordingly to the Rolls-Royce empirical correlation, similar to eq. 7, being a function of speed. These heat generation and transfer modes were applied as boundary

conditions to the ball bearing, together with the geometry and the materials properties. It is important to indicate that the specific load and the contact angle changes during the actual engine cycle, resulting in a change of conduction/convection zones and heat generation split zones around the ball raceways interface. Moreover as mentioned before the split between the different components of heat generation was kept constant at different rotational speeds. Note as well that no heat generation was applied to the cage. The model could be improved by variating the heat generation split during the cycle and including the cage.

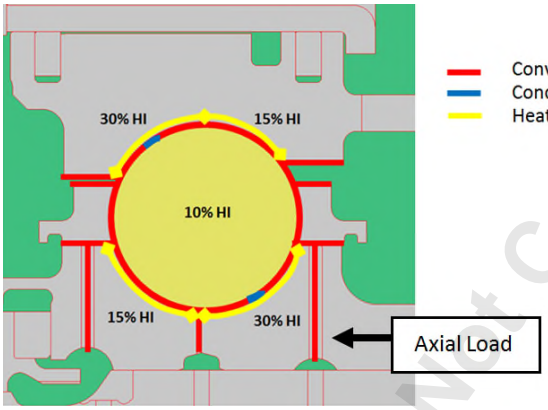

Fig. 9 Thermal BCs around the bearing

Comparison between Experiment and FEM

The temperatures measured during the experimental test have been subsequently compared with the values calculated from the FEM as a function of time and changing loads in the square cycle. These comparisons are shown in Figs 10 to 12 for thermocouples M11, M21 and M22 respectively (relative to the max measured value) and in the form of relative error in Fig 13 for all the thermocouples. It is also worth mentioning that the values at the beginning of the FEM cycle, 0 to 200s, should not be considered, in order to allow for initialization of the calculation and hence the boundary conditions are not corresponding to the actual experiment at the start. These parts have been highlighted in red in these figures.

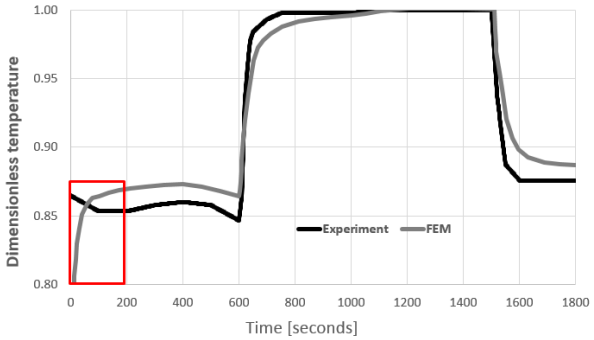

Fig. 10 Experimental and FEM dimensionless metal temperatures in M11 location

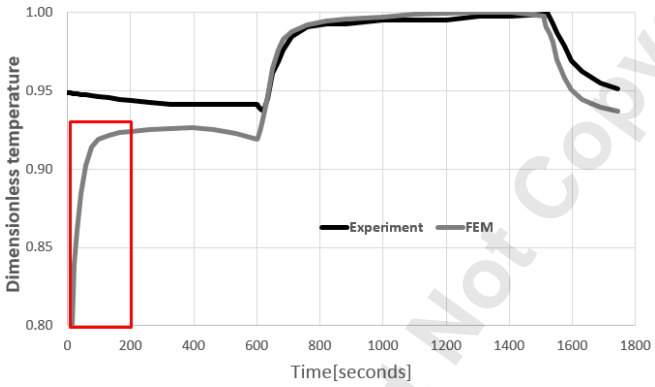

Fig. 11 Experimental and FEM dimensionless metal temperatures in M21 location

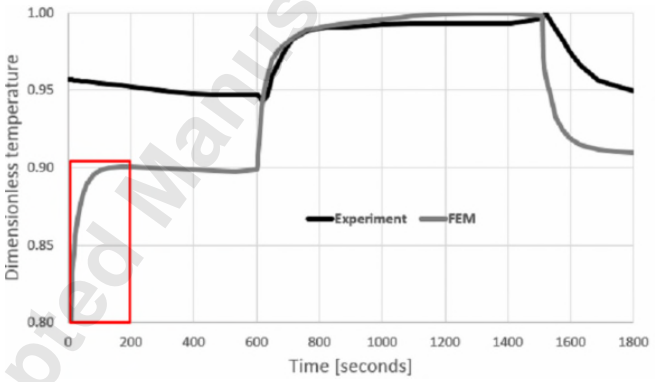

Fig. 12 Experimental and FEM dimensionless metal temperatures in M22 location

It can be observed that at M11 location the FEM model overestimates at idle, but in fact shows the overall best matching (relative error) than the other locations, as highlighted in Fig. 13. The M21 and M22 locations of closer proximity to one another show more similar trend with respects to how their respective TNM relates to its corresponding experimental values; however with larger magnitudes in the M22 location at first idle and the final idle. In comparison to M11, they overall show higher errors. Thermal exchanges on the external parts (M11) of the rings have a low impact on this

temperature which is mainly influenced by the local frictional heat generation and the heat transfer coefficient applied to the ball-raceway interfaces. On the other side location M21 and M22, inner ring, are influenced not only by the heat generation but also by the bearing feed flows.

For all three locations, the relative error is the least at high load and this is 1% and 3% when considering the lowest and highest cases (locations M11 and M22 respectively). In comparison to the TNM for which the relative peaks during acceleration, this same is observed in the FEM, with lower relative errors. One of the ways to explain this behaviour is the decision on applying a speed constant heat generation split between the balls and the cage, defined at 10% on balls surface and 90% on the contact area. Further work should be planned to verify this, in particular looking at the acceleration and deceleration where the errors present the highest values. Looking at the entire cycle, the maximum value obtained when considering all locations is under 4% (onset of deceleration) as shown in Fig 13.

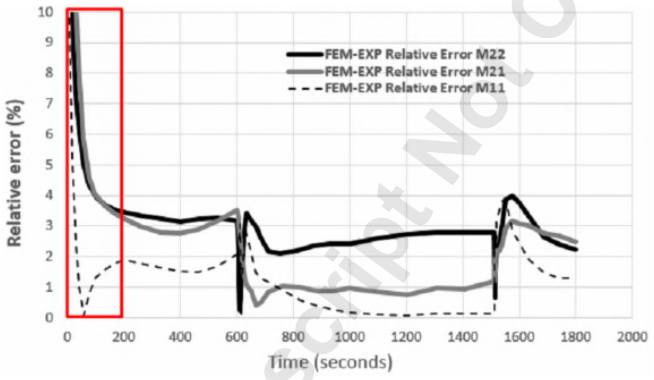

Fig. 13 Error between experimental and FEM temperatures in M11, M21 and M22 location

Limitations of the FEM

The model discussed has its constraints and hence it is only possible to extend the model to a narrow range of applications if further validations cannot be performed.

Nevertheless, most engines have similar thermal behaviours and experimental data available to check the reliability of the applied model. It was assumed that conduction and convection heat transfers are distributed based on the load path. For the same reason, the heat generation was assigned to different components and different location. However, due to the small gap between the ball and the races and its evolution during the cycle, it's hard to evaluate the correct oil mass flows and HTCs. Moreover, the changes in load magnitude and direction make the definition of the gap between the balls and race a difficult task.

Additionally the decision to apply a speed constant heat generation split between the balls and the races, defined at 10% on balls surface and 90% on the contact area, to reflect the split between the windage and the sliding

effects needs to be further investigated. Extra work is required to define these parameters for both transient and steady-state conditions.

The convective heat exchange between the lubricant and the bearing elements was derived for a single sphere that is not representative for an actual ball bearing. The effects of this assumption should be evaluated to potentially improve the methodology.

Given that the thermocouples were positioned in proximity to the ball-races interface but not on the contact zone, the effects of the boundary conditions applied around this zone can only be partially accounted for. Moreover, not all thermocouples were placed on the unloaded side where they will have provided a thermal gradient to improve the prediction of the applied boundary conditions. The test rig should be redesigned to test the validation of the assumptions with a better sensor positioning and considering variations of the oil flow in both magnitude and location.

The cages were not included into the model however the heat generated by them was included into the total heat. Future work should assess the influence of directly modelling the cage.

In the experimental bearing chamber, some cavities are fed with an air-oil mixture which is currently not part of the thermomechanical software fluid option, even though there is the capability to specify several fluids. Hence, in the case of mixed compositions in the FEM, the best practice was to set the presence of oil where it is in good proportion and specify pure air when the quantity of oil can be neglected. The consequence of this is that the heat capacity of the lubricant is better represented in the oil cavities but underestimated in the air cavities. As such, this will have an influence on convective transfer evaluation. Nevertheless, the error reached with the above threshold is acceptable. Where the heat capacity of the fluid is underestimated, the value of heat transfers coefficient is selected accordingly.

CONCLUSIONS

Throughout this paper, a revised FEM thermal modelling technique of the ball bearing is presented. A set of boundary conditions that reflect the physics of the problem is presented providing a template for predicting temperatures and heat transfers for other bearing models with limited or no experimental data for validation. The model was assessed against experimental results and with a lower order method showing better agreement in particular with a reduction of the relative error compared to the TNM of 2% at steady state and 4% during the transient. Though a close agreement between numerical and experimental results has been obtained, the high number of assumptions that had to be made, lead to a strong case-by-case dependency. A list of these assumptions has been presented underlining the need for future work to further improve the modelling of ball bearing by accuracy and robustness. Further work is suggested to improve the accuracy and confidence on the modelling technique as the flow structure is not accurately investigated in

the model; it only takes into account the overall behaviour, and it is poor in terms of local phenomena such as circulations and local vortex. Hence, to overcome this drawback, the FEM analysis could be coupled with Computation Fluid Dynamics (CFD) to better understand the complex structure of the flow and to accurately quantify the heat exchanges. Nevertheless, the use of CFD presents a significant increase in costs concerning model set up and run. Additionally, flow modulation and oil distribution should be taken into account in order to assess the validity of the method at different flow conditions. Same thing for the load applied to the bearing. Further rig tests are required.

Despite the restriction of the FEM and its scope, the boundary conditions set can be extended to other models which must be validated with appropriate experimental data before any post processes. The different boundary conditions can be maintained, but the adjustment of some coefficients may be required to reach an optimum matching.

NOMENCLATURE

a	half radius of the ellipse in the rolling direction, m
b	half radius of the ellipse in the transverse direction, m
C_p	Specific heat capacity, Jkg K
D	ball diameter, m
F_X	Axial Load
Gr	Grashof number
$h_{o.film}$	oil film convective heat transfer coefficient, W/m^{2}K
h_c	oil cavity convective heat transfer coefficient, W/m^{2}K
k	thermal conductivity of surrounding materials, W/(m K)
K	conductivity matrix, W/K
M	Specific heat matrix, J/K
N	Rotational Speed, rpm
Nu	Nusselt number
P	Vector of nodal heat flow, W
Pr	Prandtl number
R	residuals nodal heat flows, W
R	thermal resistance in/between nodes, K/W
Re	Reynolds number
t	time, s
Ta	Taylor number
$\boldsymbol{T_1}$	temperature at time 1, K
$\boldsymbol{T_2}$	temperature at time 2, K
T_{bulk}	bulk fluid temperature, K
T_{wall}	fluid temperature at the wall, K
V	speed, m/s
V_{oil}	Oil flow, l/h
x	longitudinal dimension at specified subscript,
X	Oil flow Ratio = ratio of oil through the front jet to the total oil flow in the bearing

Greek Symbol

μ	Dynamic viscosity, Pa/s
θ	time stepping coefficient
ν	Kinematic viscosity of the oil, Pas

Subscripts

12, 23, 34, 45, 56, 67, 68, 48 and 28	Between nodes 1 and 2, 2 and 3, 3 and 4…etc
a, b, c, d, e, f, g, h and i	flow path
ball	ball
int	interface
in	inlet
i.r	bearing inner ring
oil	oil
out	outlet
o.r	bearing outer ring
gap	gap

Acronyms

3D	three-dimensional
2D	two-dimensional
CFD	computational fluid dynamics
FE	finite element
FEM	finite element method
HP	high pressure
HTC	heat transfer coefficient
Hz	Hertz
IBC	isolated bearing chamber
K	Kelvin

kN	kilo Newton
kPa	kilo Pascal
kW	kilo Watt
MW	mega Watt
rpm	revolutions per minute
Q	heat transfer flow
TNM	thermal network model
W	mass flow, kg/s

REFERENCES

[1] Milman, M. and Petrick, W., 2000, "A Note On The Solution to a Common Thermal Network Problem Encountered in Heat-Transfer Analysis of Spacecraft," Appl. Math. Model., 24(12), pp. 861–879. DOI: 10.1016/S0307-904X(00)00021-4.

[2] Harris, T., 2000, "Rolling Bearing Analysis," 4th ed. Wiley-Interscience, New York, USA.

[3] Pouly, F., Changenet, C., Ville, F., Velex, P., and Damiens, B. 2010 "Investigations on the Power Losses and Thermal Behaviour of Rolling Element Bearings," Proc. Inst. Mech. Eng. Part J. Eng. Tribol., 224(9), pp. 925–933. DOI: 10.1243/13506501JET695.

[4] Hannon, W. M., 2015, "Rolling-Element Bearing Heat Transfer - Part I: Analytic Model," J. Tribol., 137(3), p. 031102. DOI: 10.1115/1.4029732.

[5] Hannon, W. M., Barr, T.A., and Froelich, S. T., 2015 "Rolling-Element Bearing Heat Transfer - Part III: Experimental Validation," J. Tribol., 137 (3), p. 031104. DOI: 10.1115/1.4029734.

[6] Rolls-Royce, 2002,"HP Ball Bearing Rig Test" Internal report.

[7] Flouros, M., 2006 "Correlations for Heat Generation and Outer Ring Temperature of High Speed and Highly Loaded Ball Bearings in An Aero-Engine," Aerosp. Sci. Technol., 10 (7), pp. 611–617. DOI: 10.1016/j.ast.2006.08.002

[8] Fénot, M., Bertin, Y., Dorignac, E., and Lalizel, G., 2011, "A Review of Heat Transfer Between Concentric Rotating Cylinders With or Without Axial Flow," Int. J. Therm. Sci., 50(7), pp. 1138–1155. DOI: 10.1016/j.ijthermalsci.2011.02.013.

[9] Holman, J.P., 2001, "Heat Transfer", 9th ed. McGraw-Hill Companies.New York, USA.

[10] Janna, W. S., 2009, "Engineering Heat Transfer," 3rd ed. CRC Press, Boca Raton FL, USA.

[11] Zienkiewicz, O. C., 1977, The Finite Element Method, 3rd ed. McGraw-Hill Book Company Ltd, UK.

[12] Edmunds,T., 1993, “Practical Three Dimensional Adaptative Analysis,” in Proceedings of the 4th International Conference on Quality Assurance and Standards, NAFEMS, Brighton, UK, May 26-28.

Transient thermal modelling of ball bearing using finite element method

Sibilli, Thierry

2017-07-11

Igie U, Sibilli T, Transient thermal modelling of ball bearing using finite element method, Journal of Engineering for Gas Turbines, Vol.140, Issue 3, GTP-16-1232, pp. 032501-1 - 032501-7
http://dx.doi.org/10.1115/1.4037861